Applied Catalysis B: Environmental 224 (2018) 136–145

Contents lists available at ScienceDirect

Applied Catalysis B: Environmental

journal homepage: www.elsevier.com/locate/apcatb

Role of CuO in the modification of the photocatalytic water splitting behavior of TiO_2 nanotube thin films

Juliana Ferreira de Brito[a,b], Francesco Tavella[a], Chiara Genovese[a], Claudio Ampelli[a,*], Maria Valnice Boldrin Zanoni[b], Gabriele Centi[a], Siglinda Perathoner[a]

[a] University of Messina, ERIC aisbl and CASPE/INSTM, Departments ChiBioFarAm and MIFT, viale F. Stagno d'Alcontres 31, 98166 Messina, Italy
[b] Institute of Chemistry-Araraquara, UNESP, Rua Francisco Degni, 55, Bairro Quitandinha, 14800-900 Araraquara, SP, Brazil

ARTICLE INFO

Keywords:
Water splitting
H_2 production
Photocatalysis
TiO_2 nanotubes
CuO nanoparticles

ABSTRACT

The role of CuO nanoparticles decorating TiO_2 nanotubes (TNT) thin film photoanodes in the behavior of photoelectrocatalytic (PEC) cells for water splitting reaction is investigated. CuO is present mainly as small nanoparticles of few nanometer decorating the internal walls of the TiO_2 nanotubes. Their presence improves i) the photocurrent behavior, ii) the H_2 generation rate by water splitting in a full PEC device (without application of a bias) and iii) the solar-to-hydrogen (*STH*) efficiency. The increase is about 20% with respect to parent TNT photoanodes using open spectrum light from a solar simulator and about 50% increase using AM 1.5G filtered light from a solar simulator. An *STH* efficiency over 2% in the full PEC cell is observed in the best conditions. *IPCE* (incident photon to current conversion efficiency) measurements clearly evidence that the presence of CuO nanoparticles induce an enhanced *IPCE* in the 300–340 nm region. The increase in the performances in water splitting is mainly associated to the transient generation of a p–n junction between the Cu_xO nanoparticles and TNT upon illumination, which enhances photocurrent density by promoting charge separation.

1. Introduction

Hydrogen production by water oxidation has received increasing interest to move towards cleaner and sustainable energy sources [1]. Hydrogen can provide a clean and safe energy storage and can be applied as an effective energy carrier for transportation and portable application. In addition, hydrogen is an important chemical for industrial processes like ammonia production, refined fossil fuels by hydrocracking and to produce different chemicals [2].

While a large variety of systems are under investigation, photoelectrocatalytic (PEC) technology for hydrogen generation is one of the most attractive routes, especially when H_2 is produced with simultaneous degradation of organic pollutants [3]. The function of a PEC device is based on the oxidation of an organic or an inorganic sacrificial agent (including water) and the reduction of water, protons or oxygen [1]. The photo-generated electrons and protons can also be used to reduce CO_2 to higher value-added liquid fuels, gaining a double environmental benefit by energy/fuel production and greenhouse gas emission reduction [4,5]. However, the development of photoanodes for practical PEC devices imposes a series of constrains that greatly limit the range of the possible materials and their characteristics. For example, it is necessary to have thin films with a specific ordered nanostructure to transport the photo-generated charges (H^+/e^-) during water oxidation to the other side of the cell, where they may combine to generate hydrogen or reduce CO_2 to fuels and chemicals [6,7]. For this reason, thin films based on an ordered array of vertically-aligned TiO_2 nanotubes still represent an important sector of development of PEC devices, even though a further engineering [8] is needed to optimize their performances. On the other hand, a great interest still exists on titania-based photocatalysts for water splitting, particularly in optimizing their behavior with visible light through different mechanisms [9–15].

Deposition of metal particles to improve the performances of titania thin films by heterojunction, co-catalysis, co-alloying or plasmonic effects has been widely investigated [16–19], with recent studies remarking also the role of one-dimensional nanoarchitecture (e.g. nanotubes) [20–23]. The synergy between one-dimensional nanoarchitecture and doping with metal nanoparticles, however, has been less investigated [15,24]. In addition, often noble metal nanoparticles (Au, Pt, etc.) have been used [25–28], while for both cost and sustainability motivations (use of non-critical raw materials) it would be preferable to use earth-abundant elements for the development of photoanodes. Among the interesting transition metals to improve semiconductor photocatalytic properties, one is copper oxide. CuO and

* Corresponding author.
E-mail address: ampellic@unime.it (C. Ampelli).

http://dx.doi.org/10.1016/j.apcatb.2017.09.071
Received 10 July 2017; Received in revised form 28 September 2017; Accepted 30 September 2017
Available online 02 October 2017
0926-3373/ © 2017 Elsevier B.V. All rights reserved.

Cu_2O are attractive due to their photoactive properties, good environmental acceptability, low thermal emittance, non-toxicity, simple and low-cost production process [29–32]. CuO is a p-type semiconductor that absorbs light in the visible spectral region, evidencing a bandgap energy between 1.2 and 1.7 eV [33]. Copper oxides are good materials for junctions due to their ability to act simply as an electron trap. Moreover, the electrons have to be consumed in some way, otherwise there will be an accumulation of charge on the surface [34]. Recently, some authors studied the modification of TiO_2 nanotubes with copper oxides (CuO and Cu_2O) and metallic copper in order to improve the photo-response of the system [35–37]. It should be commented, however, that while Cu_2O is interesting for the possibility to promote by semiconductor–semiconductor junction the visible-light response, the stability of this reduced species under the strong oxidizing conditions of the photoanode (nascent oxygen) is questionable. The role of CuO nanoparticles is also unclear. Teng et al. [38], studying Pt@CuO/TiO_2 photocatalysts, but testing in methanol/water solution under UV-light irradiation, indicated that stable p–n heterojunctions form at the interface between CuO and TiO_2 nanosheets, owing to the strong interaction of CuO with the {001} facets of the TiO_2 sheets. This effect decreases the recombination rate of electrons and holes. Hua et al. [39] indicated that CuO reduces to Cu_2O during the initial stage of photocatalytic reaction, and the latter is responsible for the improved photocatalytic activity. However, tests were made in a 10% aqueous solution of methanol, and thus the reduction of copper is likely induced by the organic solvent oxidation. Xu et al. [40] observed a high activity of TiO_2 nanotubes decorated with CuO nanoparticles, but again testing behavior was evaluated in a 10 vol% methanol-water mixture. No indication has been given about the physico-chemical role of copper oxide nanoparticles in promoting the behavior. Ho et al. [41] studied ternary hybrid TiO_2/CuO/Cu materials and indicated that the heterojunctions among the TiO_2, CuO, and Cu interfaces enhance the space separation and transfer of the photogenerated charge carriers. Even in this case, tests were made in water-methanol solution. Yu et al. [42] investigated CuO-deposited TiO_2 rod composites again in water-methanol mixtures. They interpreted the promotion effect of CuO in general terms of synergistic effects of high surface area, specific energy band structure, and enhanced light harvesting at the interface of CuO and porous TiO_2 rods. Kumar et al. [43] studied CuO–TiO_2 nanocomposites in a water–glycerol mixture indicating that CuO nanoparticles facilitate the charge separation and electron transfer.

This short survey of recent results on CuO-TiO_2 photocatalysts evidences the lack in understanding the behavior of these materials without the presence of sacrificial agents (organic molecules) and about the specific role of CuO in promoting the behavior in water splitting of titania thin film photoanodes based on TiO_2 nanotube ordered arrays. This study is thus focused at these aspects to develop advanced photoanodes for solar photo-electrochemical reactors [44–46] for sustainable production of hydrogen by water splitting or CO_2 reduction to fuels/chemicals using light as power supply.

The water splitting reaction, in addition, was studied in a compact PEC solar cell characterized by the photoanode and the cathode joint on the two sides, respectively, of a Nafion® thin proton membrane. This PEC solar cell design represents a state-of-the-art for practical development of this type of cells, with production of H_2 and O_2 in separate compartments, continuous operations, minimization of electrolyte volume, easy scale-up and sealing, possibility of operations either in water splitting or CO_2 reduction [45]. Many literature results in H_2 photoproduction, besides to use sacrificial agents (as indicated above for CuO-TiO_2 photocatalysts), are made in slurry photoreactors without separating H_2/O_2 production, or in PEC reactors with characteristics very different from those required for practical implementation. The results reported here, thus, refer to performances obtained under relevant experimental conditions (no extra bias, no sacrificial donors used, easy separation of products) for utilization of nanostructured TiO_2-based photoanodes modified with non-noble metal/metal oxide (such as CuO and Cu_2O) in order to increase their photocatalytic efficiency in PEC water splitting for a sustainable production of clean and renewable hydrogen.

2. Experimental

2.1. Synthesis

TiO_2 nanotube (TNT) array electrodes were prepared as earlier described [8]. Briefly, titanium plate (Alfa Aesar, 0.025 mm of thickness, 3.5 cm of diameter) was cleaned by 30 min sonication with isopropanol at 40 °C and then with ultrapure water. Electrochemical anodization was performed in a two-electrode cell using platinum as counter-electrode and a solution of ethylene glycol with 0.3% ammonium fluoride and 2.3% water as supporting electrolyte. The applied potential was initially ramped from 0 to 50 at 5 V min^{-1} and then kept constant at 50 V for 1 h. After the anodization, the electrode was cleaned by sonication with a 37% HCl solution (1 min) and annealed at 450 °C for 3 h. A thin Ti layer remained non-oxidized, thus acting as an electron-collective layer in the PEC experimental apparatus.

The TNT thin films were decorated with CuO nanoparticles (CuO-TNT) by dip coating using an adapted methodology [47]. The solution used for dip coating was prepared with copper nitrate hydrate (8.4×10^{-3} mol L^{-1} of metal) as copper oxide precursor, citric acid and ethylene glycol in molar ratio of 1:4:16, respectively. The electrode, after drying, was annealed at 450 °C for 3 h.

2.2. Characterization

Field emission scanning electron microscopy (FE-SEM) images were recorded using a Zeiss model Supra 35 equipped with an energy dispersive X-ray (EDX) spectrometer. High resolution transmission electron microscopy (TEM) images were recorded using a CM200 transmission electron microscope (TEM) (Philips/FEI, Netherlands) operated at 200 kV.

The total copper concentration was evaluated by atomic absorption spectroscopy (AAS) using an AAnalyst 200 spectrometer by PerkinElmer. For the analysis, the CuO-TNT sample was sonicated in concentrated HF aqueous solution (48 wt%) to dissolve Cu and the resulting solution was analyzed after proper dilution. The calibration curve was obtained by means of three standard solutions in the range 1–5 ppm by diluting Copper Standard for AAS (1000 mg L^{-1} in nitric acid) supplied by Sigma Aldrich.

X-ray diffraction patterns were recorded on a Bruker Model D2 Phaser.

X-ray photoemission spectra were collected using PHI VersaProbe II analyzer. Cu_{2p} binding energies (BE) were recorded using AlKα (1486.6 eV) as the excitation source and a pass energy of 23.5 eV. The XPS spectra were recorded with setting of 100 µ100W20kv_HP. Position of XPS peaks of the corresponding element is referred to the C_{1s} peak of carbonaceous contamination, whose energy is taken equal to 284.80 eV.

An UV/Vis spectrometer (Jasco V-570PerkinElmer Lambda 1050) was used for diffuse reflectance measurements in order to obtain the optical band gap.

The photocurrent response was evaluated by linear sweep voltammetry in 1.0 mol L^{-1} Na_2SO_3 using a scan rate of 100 mV s^{-1} obtained by using a potentiostat/galvanostat (AMEL 2049).

2.3. H_2 production by water splitting

The water splitting was carried out using a photo-electrochemical reactor made of Plexiglas and equipped with a quartz window. It has a two-electrode configuration with two compartments for separated evolution of H_2 and O_2 [8,44,48]. The photoanode consisted of the TiO_2 nanotubes with CuO nanoparticles supported over the Ti foil, while the

cathode was a commercial carbon gas diffusion layer (GDL) loaded with Pt (0.5 $mg_{Pt}\ cm^{-2}$, GDE S10BC SIGRACET®, supplied by Ion Power). The two electrodes were joint together by a Nafion® membrane. 1 mol L^{-1} NaOH and 0.5 mol L^{-1} H_2SO_4 were used as supporting electrolytes in the anodic and cathodic compartments, respectively. Each solution circulated continuously between the solar cell and an outer reservoir. A potentiostat/galvanostat (AMEL 2049) was used to measure the generated photocurrent. The solar illuminator used for the experiments was a Xe arc lamp (ORIEL, 300 W) equipped with a set of lenses for light collection and focusing, a water filter to eliminate the infrared radiation and a set of filters to evaluate the photo-response in different light-absorption regions (ultraviolet or visible regions). The irradiated area was 5.7 cm^2. H_2, O_2, CH_4 and CO amounts in the gas streams were determined by an on-line gas-chromatograph (GC) (Agilent Technologies 7890A) using a column 5A Plot permanent gases (Restek®). Helium was used as carrier gas at 1.0 mL min^{-1} flow rate.

The solar-to-hydrogen (*STH*) efficiency in the PEC cell was calculated by the formula:

$$STH = \frac{R_{H2}{}^{*}\Delta G^{0}}{Ptot^{*}A} \quad (1)$$

where R_{H2} is the rate of hydrogen production (mol·s^{-1}), ΔG^0 is the standard Gibbs energy at standard conditions (2.372×10^5 J mol^{-1}), P_{tot} is the light irradiance (W cm^{-2}) and A is the irradiated area of the photocatalyst (cm^2).

The incident photon to current conversion efficiency (*IPCE*), i.e. a measure of the effectiveness in converting incident photons on the cell to photocurrent flowing between the working and counter electrodes, was calculated by the following equation:

$$IPCE\,(\%) = 1240\frac{I_p(\lambda)}{P_{inc}(\lambda)\lambda}{}^{*}100 \quad (2)$$

where $I_p(\lambda)$ is the photocurrent density (A m^{-2}) and $P_{inc}(\lambda)$ is the incident power density of light (W m^{-2}) at wavelength λ (nm). The constant "1240" has the unit W nm A^{-1}. An *IPCE* of 100% means that all the photons generate electron–hole pairs, but in practical situations *IPCE* values are less than 100% due to the losses corresponding to the reflection of incident photons, their imperfect absorption by the semiconductor and recombination of charge carriers within the semiconductor. *IPCE* is usually calculated by measuring the current in the cell, when a particular wavelength or a small group of wavelengths with a known power density $P_{inc}(\lambda)$ are incident on it. The IPCE was calculated without the application of a potential between the two electrodes ($V_{bias} = 0$) and the measured photocurrent density $I_p(\lambda)$ was the result of the solely absorbed photons by the semiconductor without any external applied bias.

3. Results

3.1. Physico-chemical characteristics

Fig. 1 shows the FE-SEM images of TNT and CuO-TNT samples. The top view (Fig. 1a) indicates the presence of well-ordered TiO_2 nanotubes with wall thickness ranging from 20 to 27 nm and internal nanotube size in the 40–55 nm range. The copper oxide was deposited around the TiO_2 nanotube wall, as it can be observed by the increment in the wall thickness that ranges from 27 to 36 nm after CuO deposition (Fig. 1b). CuO nanoparticles are present mainly within the titania nanotubes, except a few CuO nanoparticles with size between 18–33 nm present on top of the TiO_2 nanotubes as evidenced by FE-SEM images with higher magnification (Fig. 1c and d). The effective Cu loading in CuO-TNT sample, analyzed by AAS, was about 9 wt.%.

Fig. 2 reports XRD and EDX results for CuO-TNT sample. Fig. 2a shows the XRD pattern confirming the presence of crystalline anatase TiO_2 phase and CuO crystallites, in addition to the background signal of Ti relative to the metallic titanium substrate of the electrode, which the TNT thin film was grown on. With respect to relative intensities of reflections in TiO_2 anatase (JCPDS 88–1175), the reflections corresponding to (002) plane are slightly intensified with respect to the more intense (101) reflection. This corresponds to TiO_2 crystals slightly elongated along this crystalline plane and exposing preferentially {001} facets [49]. The XRD of CuO phase corresponds instead to that expected for CuO nanoparticles with monoclinic structure [50]. Fig. 2b shows the EDX analysis, confirming the presence of Ti, Cu and O.

Fig. 3 shows the XPS spectrum of CuO-TNT sample, evidencing the Cu $2p_{3/2}$ and Cu $2p_{1/2}$ peaks at 933.5 eV and 952.4 eV, respectively, which can be ascribed to the presence of CuO [51,52]. However, the signals related to Cu_2O are not visible, probably because only a few Cu_2O nanoparticles are present and they are mainly localized inside the TNT nanotubes, due to the method of preparation.

Fig. 4a reports a high resolution TEM image of the CuO-TNT sample, evidencing the presence of a TiO_2 nanotube with small CuO nanoparticles of about 2 nm decorating the internal walls of the nanotube (one of the particles is indicated with an arrow). It is also possible to observe in Fig. 4b the presence of titania nanosheets with distance of 3.63 Å plane (101) as expected, as well as the presence of CuO from the lattice spacing of plane (111) measured as 2.43 Å.

Fig. 5a reports the UV–vis region spectra of TNT and CuO-TNT electrodes. The spectra are characterized by a strong adsorption below 400 nm, related to the typical band gap of TiO_2, and a broad adsorption between 500 and 1200 nm, with a maximum at about 700 nm for TNT and shifted to about 800–900 for CuO-TNT. The latter adsorption, however, is related to a physical light scattering effect (photonic behavior) and in part to interference patterns arising from wavelength-dependent constructive and destructive interference of partially reflected light in the thin films [53]. The change in this part of the spectrum is related to the increased wall thickness of TiO_2 nanotubes due to decoration with CuO, as commented above.

Fig. 5b presents the band gap energy for the materials obtained by Tauc's graphic [54] using Kubelka-Munk function, according to the Eq. (3) below:

$$\alpha = (1 - R)^{1/\gamma}/2R \quad (3)$$

where α is the material absorptivity and R being the reflectance. The γ was assumed as two (indirect electronic transition allowed) once this is the electronic transition more suitably indicated for both the TiO_2 [55] and CuO [56]. The band gap for TiO_2 nanotubes (3.2 eV) corresponds to that typically reported for anatase TiO_2 [57]. A shift in the band gap energy to around 2.8 eV was observed for CuO-TNT. However, the clear tail in the absorption edge of band gap is an indication of the presence of Cu_2O nanoparticles, evidencing an additional band gap energy of about 2.0 eV (see the dashed red line in Fig. 5b), in accordance with what reported in literature for Cu_2O [58].

Besides the band gap, the knowledge of the position of the band edges is a crucial prerequisite for understanding the photo-activity of a semiconductor. The position of the conduction band (CB) edge for pure anatase TiO_2 is at about −0.37 V (vs. NHE) [59]. The presence of Cu-based nanoparticles on TiO_2 influences the CB edge depending on Cu loading. For 10 wt.% Cu on TiO_2, the location of the CB edge diminishes to about −0.22 V [60]. The standard redox potential for the couple H^+/H_2 (pH = 0) is zero (vs. NHE), but it becomes −0.83 eV at pH = 14, as in the PEC system the photo-electrode operates in an aqueous solution of NaOH (1 M). In order to have water reduction to H_2, the CB of the composite material should be more negative than the redox potential for the couple H^+/H_2, thus the testing conditions seem to be unfavorable (−0.22 vs. −0.83 V). However, due to the design of the PEC cell, water reduction does not occur at the photoanode, but electrons are collected at the bottom metallic layer of the electrode (Ti not oxidized during the anodic preparation) and transferred to the cathode side (H_2SO_4 0.5 M, redox potential H^+/H_2 = ~0 V) where they combine with protons coming from the Nafion® membrane to form hydrogen. Thus, in this configuration the position of the CB edge (about

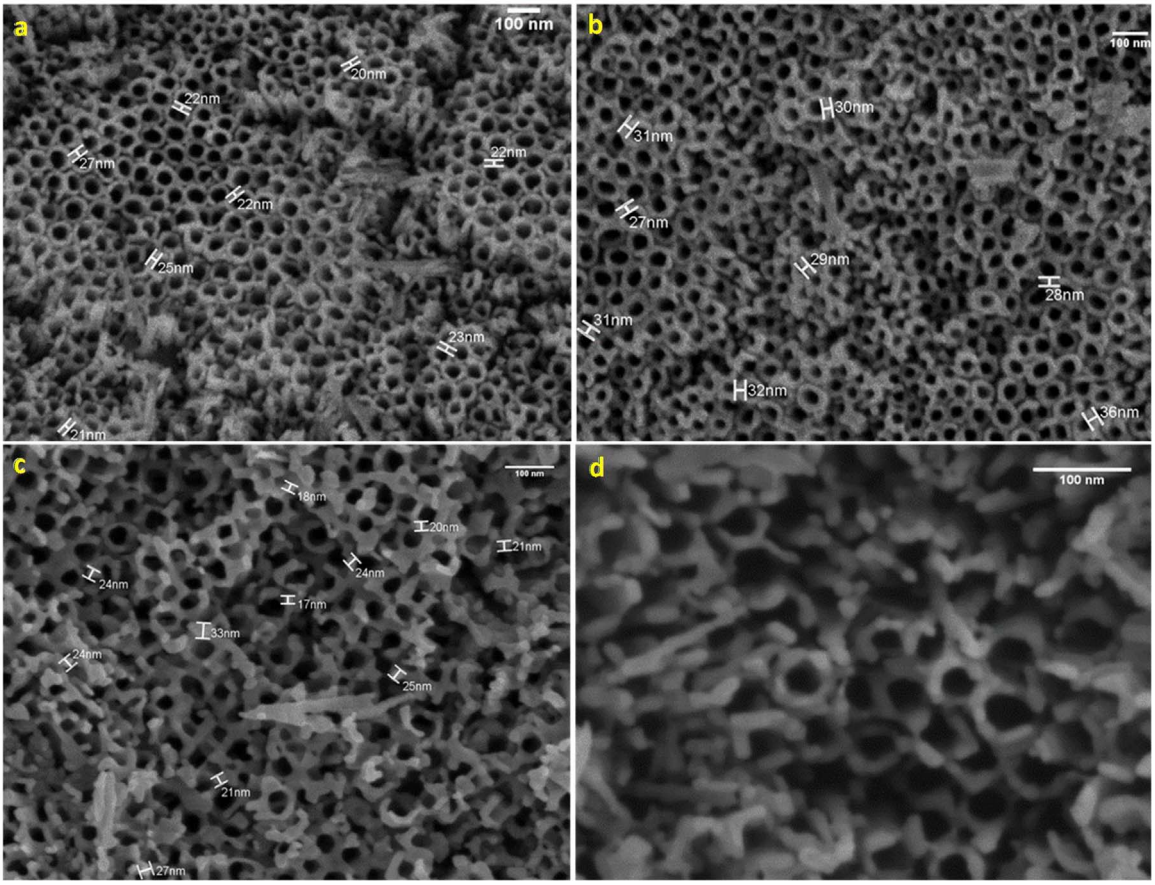

Fig. 1. FE-SEM image of TiO_2 nanotubes without modification (a) and TiO_2 nanotubes decorated with CuO nanoparticles at 50000 (b), 100000 (c) and 200000 times (d) of magnification.

−0.22 V for 10 wt.% Cu nanoparticles on TiO_2) with respect to the redox potential H^+/H_2 half-reaction (E = 0 vs. NHE) is thermodynamically favorable for water reduction, because the half-reaction occurs in the other compartment (cathode). On the contrary, the position of the valence band (VB) edge (it is of fundamental importance for water oxidation) must be more positive than the redox potential of the couple O_2/H_2O or O_2/OH^- (+1.23 eV at pH = 0, but the redox potential diminishes to +0.40 eV at pH = 14). As the measured band gap of CuO-TNT sample is 2.8 eV, the position of the VB edge can be calculated by subtracting 0.22 from the band gap. The result is that the VB edge is located at +2.58 V, which is more positive than the redox potential of the couple O_2/OH^- at pH = 14 (+0.40 eV), making water splitting process thermodynamically favorable in our PEC cell.

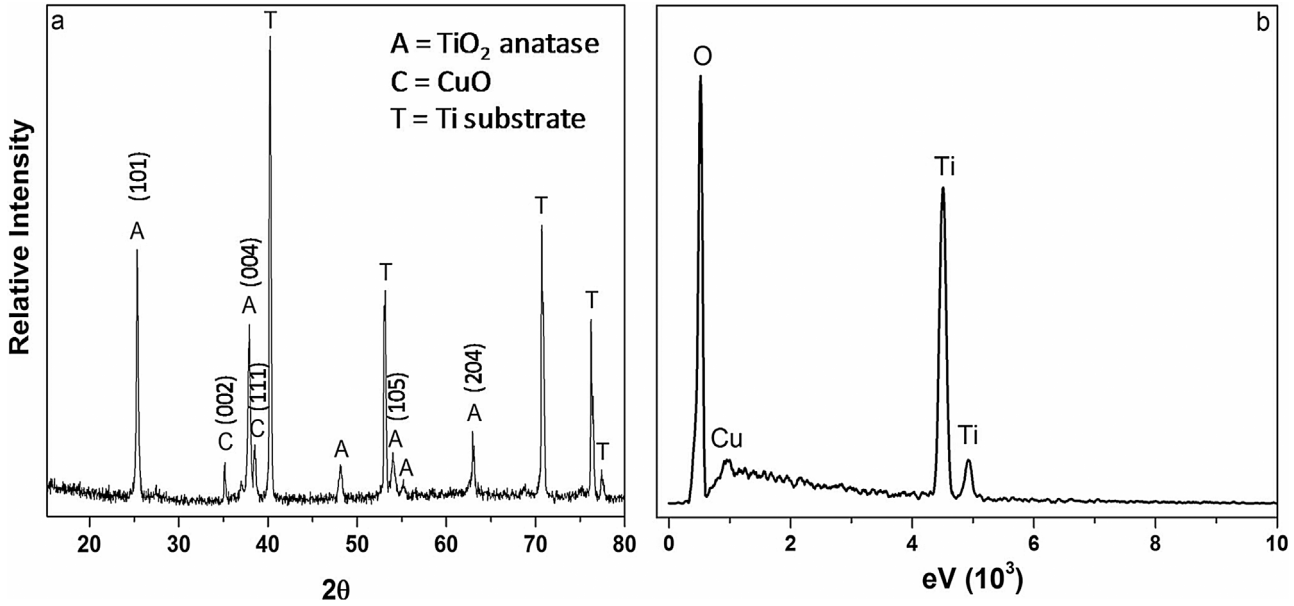

Fig. 2. CuO-TNT: a) XRD pattern where A represents anatase phases of TiO_2, T represents the metallic titanium used as substrate and C represents the CuO peaks and b) EDX spectrum.

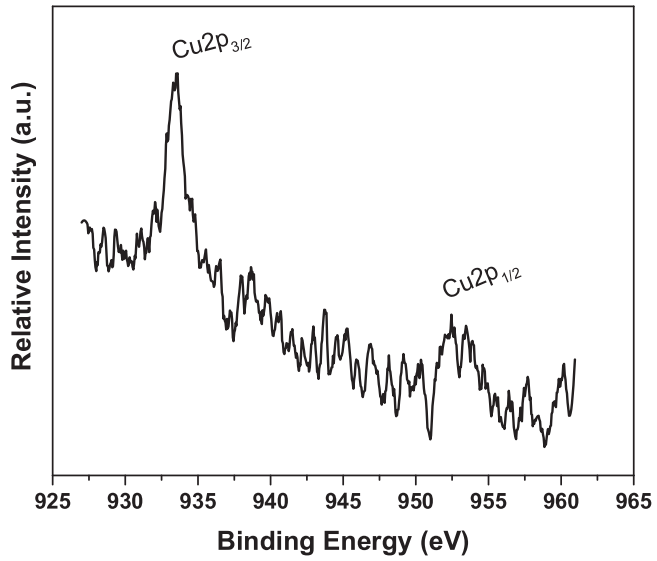

Fig. 3. X-ray photoemission spectrum of CuO-TNT sample, showing Cu $2p_{3/2}$ and Cu $2p_{1/2}$ peaks related to CuO.

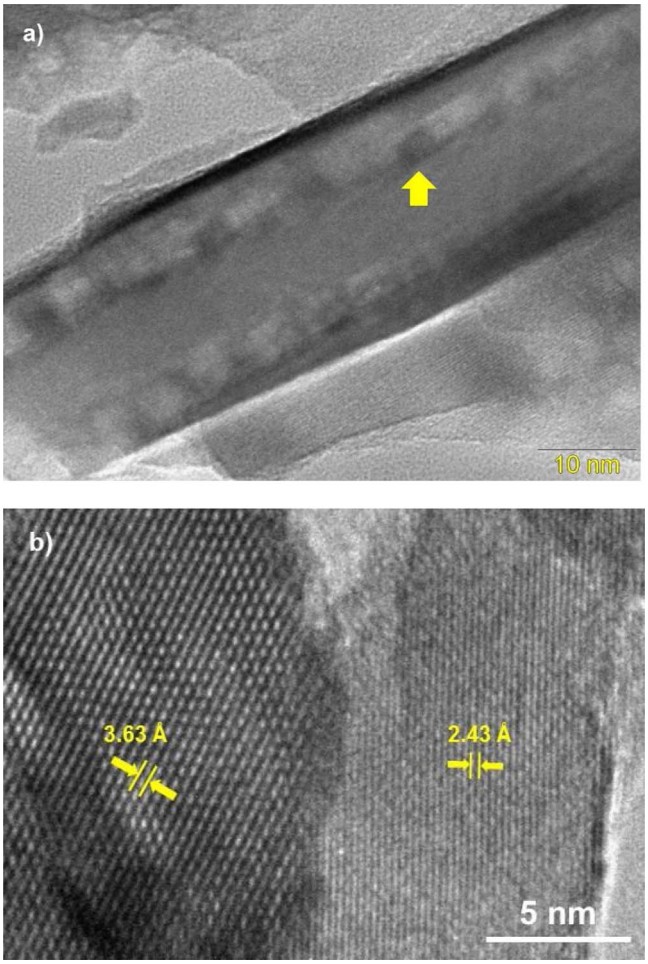

Fig. 4. TEM images of CuO-TNT sample showing: a) a TiO_2 nanotube decorated in the internal walls with CuO nanoparticles (one evidenced by an arrow) and b) the lattice planes of TiO_2 and CuO.

3.2. Photo-current performances

The photo-current performances were evaluated with chronoamperometric measurements using a three-electrode cell with 1.0 mol L^{-1} Na_2SO_3 as the supporting electrolyte and an open and close light incidence system with and without filter AM 1.5 G (simulating standard terrestrial solar irradiance distribution). The results are presented in Fig. 6a. Being the filtered light reducing the number of photons reaching the electrode, the results in Fig. 6a have been normalized for 0.1 W cm^{-2} incident light irradiance. Fig. 6b shows an expansion of one of the chronoamperometric cycles to evidence better the differences between TNT and CuO-TNT samples. As reference, Fig. 6c reports the irradiance for open spectrum and AM 1.5 G filtered light from solar simulator.

Several indications derive from these studies. The first is the general good photocurrent of these samples with stable and reproducibility behavior in several consecutive chronoamperometric cycles. CuO-TNT samples show about 27% increase in normalized current density with respect to TNT with open spectrum and about 42% increase with AM 1.5G filtered light, even if the normalized current density in the latter case is about 23% of that of open spectrum. Fig. 6c reports the irradiance of the incident light for open spectrum and AM 1.5G light. The latter cut essentially the light component before 350 nm. Thus, about 75% of the photocurrent density derives from the light component below about 350 nm. Nevertheless, above this threshold, roughly corresponding to the band gap in TiO_2, still a quarter of the open spectrum normalized photocurrent density is present. The decoration of TNT with CuO leads to an enhancement of the normalized photocurrent density both with open spectrum and AM 1.5G filtered light, more intense in the latter case (42% increase with respect to 27% enhancement).

As better remarked in the expansion of one of the cycles in open spectrum chronoamperometric tests (Fig. 6b), there is a further difference between TNT and CuO-TNT. In the former case, there is a fast increase and decrease in the photocurrent density on switching on/off the light. On the contrary, in CuO-TNT, the current density reaches quickly about 85% of the maximum value, and then slowly further increases in the next 30–40 s up to reaching a constant value. The effect is well reproducible in consecutive cycles. When light is switch-off, there is instead a tail in reaching the background value in the case of CuO-TNT. The effect is not present in the case of AM 1.5G filtered light. The effect can be interpreted as a trapping of part of the electrons with sufficient energy in heterojunctions created at the CuO-TNT interface, which leads to a partial delay in reaching steady current density. These trapped electrons are then released during switching off the light and are responsible for the tail.

3.3. H_2 production by water splitting

The behavior of the TNT and CuO-TNT photoanodes in water splitting reaction was studied in a compact PEC solar cell as indicated in the introduction. The TNT or CuO-TNT photoanodes were used as working electrodes and a commercial gas diffusion layer (GDL) loaded with Pt was employed as counter electrode. In this type of cell, the photoanode (upon illumination) generates electron and hole pairs, which are transported in the thin film to the bottom of the TNT film supported over a microholed Ti thin layer acting as electron collector. The protons pass through the microholes and then reach the Nafion® membrane located on the other side of the Ti thin layer. They pass through the Nafion® membrane and reach the cathode (Pt nanoparticles supported on GDL), where then react with electrons (transported through an external wire) to generate H_2. 1.0 mol L^{-1} NaOH is used as supporting electrolyte in the anode compartment and 0.5 mol L^{-1} H_2SO_4 supporting electrolyte in the cathode compartment. No external bias is applied. Stable current density is observed in these tests (Fig. 7), with the current density higher for the case of CuO-TNT with respect to TNT, in agreement with what observed in chronoamperometry studies (Fig. 6). The small spikes observed in the current density are related to H_2 or O_2 bubbles formation. The initial change in current density during about the first 10–15 min is related to the establishment of equilibrium in the PEC solar cell upon the start of the

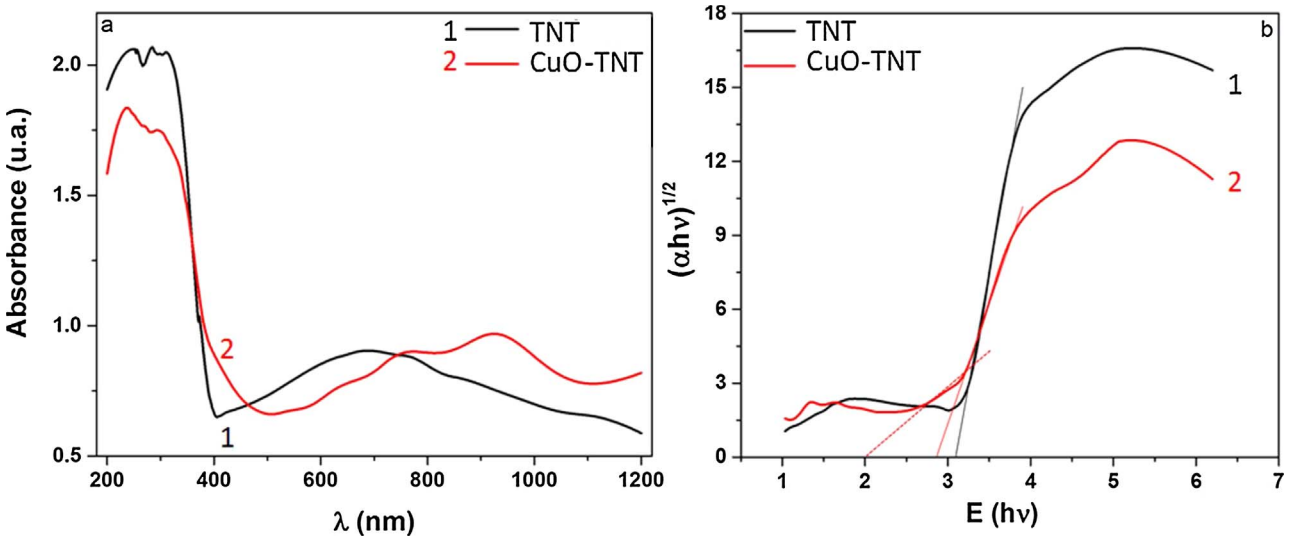

Fig. 5. a) Diffuse reflectance spectrum in the UV–vis region of TNT (black line) and CuO-TNT (red line) and b) band gap energy calculated by Kubelka-Munk for TNT (black line) and CuO-TNT (red line). The dashed red line indicates an additional band gap edge related to Cu_2O. (For interpretation of the references to colour in this figure legend, the reader is referred to the web version of this article.)

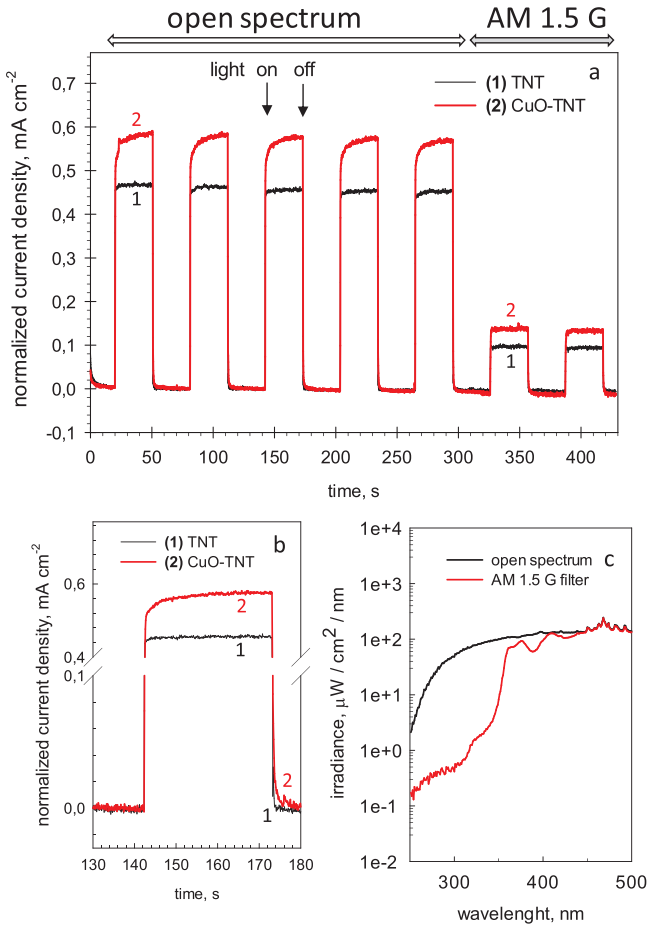

Fig. 6. a) Chronoamperometric measurements for TNT and CuO-TNT samples (0.1 V vs. Ag/AgCl, 1 M Na_2SO_3) using open spectrum and AM 1.5G filtered light of a solar simulator. The data were normalized for 0.1 W cm^{-2} incident light irradiance. b) Expansion of one of chronoamperometric cycles. c) Irradiance for open spectrum and AM 1.5 G filtered light from solar simulator.

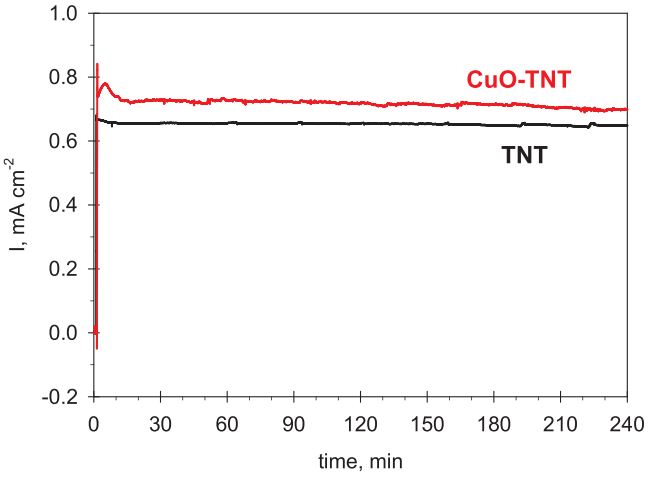

Fig. 7. Current density generated applying open spectrum solar simulator light to TNT and CuO-TNT photoanodes in the compact PEC solar cell.

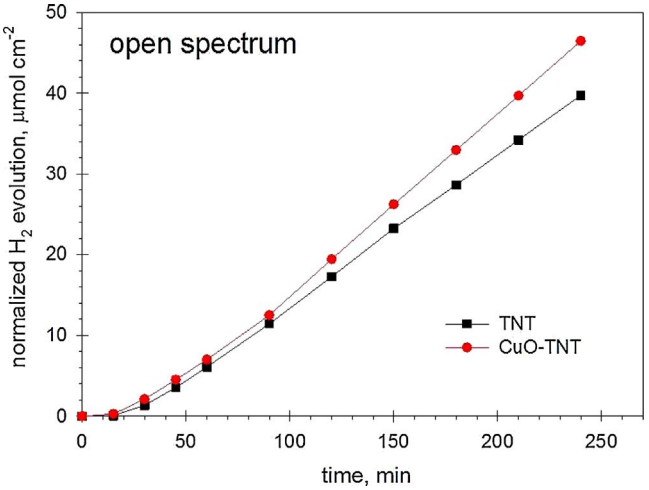

Fig. 8. Cumulative hydrogen formation as a function of time from the cathode of the PEC cell using TNT or CuO-TNT as photoanodes in tests with not-filtered light (open spectrum from the lamp) of a solar simulator. The data were normalized for 0.1 W cm^{-2} incident light irradiance.

illumination.

Fig. 8 reports the cumulative H_2 formation as a function of time in the compact PEC solar cell using TNT or CuO-TNT as photoanodes in tests with not-filtered light (open spectrum from the lamp) of a solar simulator. As commented for chronoamperometry tests, the data were normalized for 0.1 W cm^{-2} incident light irradiance. The initial apparent induction time is related to the establishment of the equilibrium in the PEC solar cell, as commented above. Note that H_2 evolves at the cathode (Pt/GDL electrode), but the change in the photoanode (TNT, CuO-TNT) determines a different rate of photogeneration of H^+/e^-.

There is a stable continuous production of H_2 for both TNT and CuO-TNT photoanodes within the investigated time period (about 4 h), indicating no deactivation. A parallel O_2 evolution from the other cell compartment, according to stoichiometry, was observed. Whereas an apparent increase in the rate of H_2 production from the first period (30–90 min) to the period from 90 to 250 min was detected, but this is related to establishment of equilibrium in the PEC cell. After about 90 min the rate of H_2 production (normalized for 0.1 W cm^{-2} incident light irradiance) is stable and equal to 11.32 and 13.64 μmol_{H2} cm^{-2} h^{-1} for TNT and CuO-TNT, respectively. The rate is about 20% higher for CuO-TNT photoanode, which well corresponds to the increase in photogenerated current density determined either in-situ or in the separated chronoamperometry tests (Fig. 6).

A direct comparison of these results with literature is not possible, because the data on comparable photoanodes were obtained using sacrificial agents or using not comparable cells. We earlier reported [61] for comparable photoanodes and PEC cells the H_2 production using TiO_2 nanotubes doped with metallic Cu and Au nanoparticles. The H_2 formation observed were 0.87 μmol min^{-1} with metallic Cu and 0.98 μmol min^{-1} with metallic Au nanoparticles decorating the TNT films. Comparing these rate of H_2 photoproduction with the results presented here (Fig. 8) it may be observed that the doping of TiO_2 nanotubes with copper oxide improves of about 54% the H_2 production, being the reaction rate for CuO-TNT about 1.34 μmol min^{-1} for a similar photoanode size.

The results in normalized H_2 photogeneration in a PEC cell using TNT and CuO-TNT photoanodes and AM 1.5G filtered solar simulator light are reported in Fig. 9. Here the apparent induction time is slightly longer, but this is related to the lower amount of H^+/e^- photogenerated. The normalized rates of generation of H_2 (after the initial time of about 90 min) are 1.56 and 3.43 μmol_{H2} cm^{-2} h^{-1} for TNT and CuO-TNT, respectively (normalized for 0.1 W cm^{-2} incident light irradiance). In this case, CuO-TNT shows about 120% increase in the H_2 production rate with respect to TNT. This is more than twice the

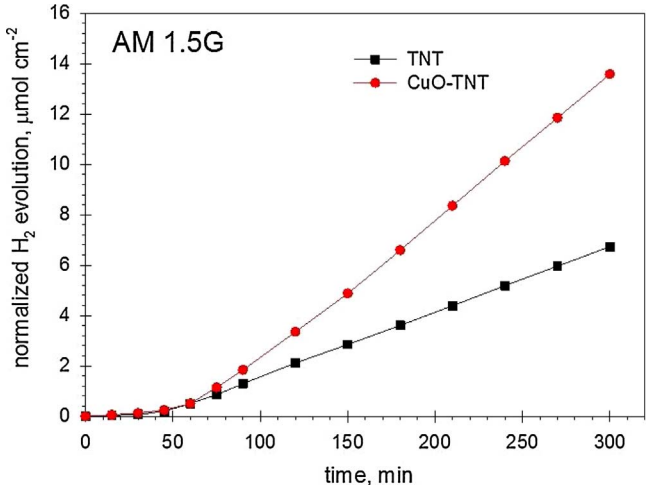

Fig. 9. Cumulative hydrogen formation as a function of time from the cathode of the PEC cell using TNT or CuO-TNT as photoanodes in tests with AM 1.5G filtered light of a solar simulator. The data were normalized for 0.1 W cm^{-2} incident light irradiance.

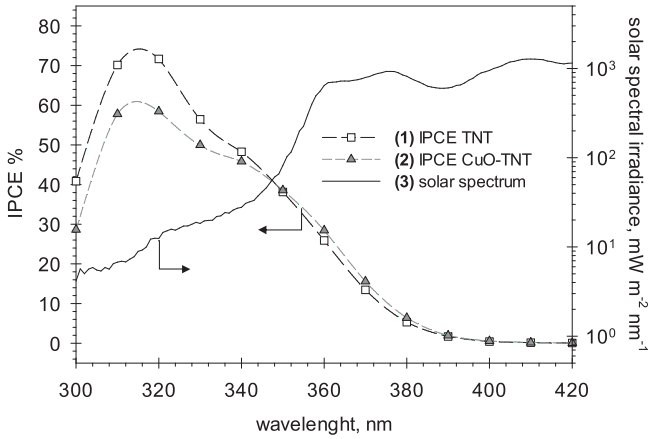

Fig. 10. Incident photon to current conversion efficiency (*IPCE*) spectra of TNT and CuO-TNT photoanodes tested in the PEC cell. The solar simulating spectral irradiance vs. wavelength is also reported. The slit width is 4 mm.

increment observed in current density (about 50%) observed during these tests and in chronoamperometric experiments (Fig. 6). However, the normalized H_2 production rate for CuO-TNT using AM 1.5G filtered light is about 25% of that measured for open spectrum, in well agreement with the observed normalized decrease in photocurrent generation for open spectrum and AM 1.5G filtered solar simulator light during chronoamperometric tests (Fig. 6).

3.4. Incident photon to current conversion efficiency

Further insights on the effect of CuO in modifying the properties of TNT photoanodes in water splitting reaction in a PEC solar cell derive from the analysis of the incident photon to current conversion efficiency (*IPCE*). The results are shown in Fig. 10. *IPCE* is a measure of the effectiveness in converting incident photons on the cell to photocurrent flowing between the working and counter electrodes. *IPCE* is also called the external quantum efficiency. The presence of CuO nanoparticles decorating the TiO_2 nanotubes slightly increases *IPCE* in the 350– 390 nm spectral region, while it has essentially zero effect at higher wavelengths.

3.5. Solar-to-hydrogen efficiency

Solar-to-hydrogen (*STH*) efficiency, i.e. the ratio between the maximum energy output that can be obtained from the final products (hydrogen) and the energy supplied (in the form of light energy), is perhaps the most relevant result for practical uses, together with stability, cost-effectiveness in preparation and scale-up. For example, submicrometer CoO octahedrons are reported to have between the highest *STH* values (about 5%), but have problems of stability (photothermal-induced CoO to Co_3O_4 transformation in the presence of oxygen and water, even if the support over graphene can improve stability) and were tested only in powder and not in the form of a thin film in a PEC device [62]. Multijunction PV cells modified with hydrogen evolution reaction (HER) catalysts have been reported to arrive to about 8% *STH* [63], but without the separation of the produced H_2 and O_2, which in turn creates problems of safety and costs of separation. In addition, a very complex multilayer solar cells (a-Si:H/a-Si:H/μc-Si:H cell, deposited on TCO coated glass, with ZnO:Al/Ag as back contact/reflector; in total 13 layers) is required with issues in costs, stability and scalability. For PEC cells and materials closer in characteristics to those reported here, it may be cited, for example, recent results obtained with $BiVO_4$ photoanodes reporting an *STH* efficiency of 0.57% (corresponding photocurrent density of 0.46 mA cm^{-2}) under AM 1.5G illumination (100 mW cm^{-2}) [64]. Co doped ZnO nanowires show an *STH* of 0.06% for an applied potential of 0.8 V [65] using not-filtered light.

Table 1
H_2 production rate and solar-to-hydrogen *(STH)* efficiency for PEC cell using TNT and CuO-TNT photoanodes.

Photoanode	*Incident light*	*H_2 production rate ($\mu mol\ h^{-1}$)*	*STH efficiency (%)*
TNT	Open spectrum	85.5	1.68
TNT	Solar (AM 1.5G)	7.8	0.24
CuO-TNT	Open spectrum	104.3	2.04
CuO-TNT	Solar (AM 1.5G)	17.4	0.53

A photoanode based on a thin hematite film exhibiting solely (110) crystal orientation shows an *STH* of 0.04% at a potential applied of about 1.15 V and using AM 1.5 G filtered light source of 100 mW cm^{-2} intensity [66]. These indications, although not exhaustive (further indications are given in the review by Chen et al. [67]) evidence that except for multijunction PV cells, for which remarks about costs, stability and practical scalability exist, the reported *STH* efficiencies are often below 1% using not-filtered light and below 0.1% using AM 1.5G filtered light.

These considerations are necessary to evaluate better the *STH* results of TNT and CuO-TNT photoanodes (Table 1), taking in consideration also that these results are obtained in a full PEC device without external applied bias, and not by evaluating the photoanode under bias application as in various of the results cited above. The *STH* efficiency of TNT is 1.68%, which increases to over 2% for CuO-TNT sample (about 20% increase) using not-filtered light (open spectrum) from the solar simulator. Using AM 1.5G filtered light the *STH* efficiency is lower, and increases from 0.24% to 0.53% in passing from TNT to CuO-TNT. These values of *STH* efficiency are high in comparison with literature results on comparable systems and experimental conditions, as commented above.

4. Discussion

The deposition of CuO nanoparticles in TNT thin films leads to photoanodes with improved photocurrent behavior, improved behavior in H_2 generation by water splitting in a full PEC device (without application of a bias) and improved *STH* efficiency. The increase is of about 20% with respect to the parent TNT photoanode using open spectrum light from a solar simulator and about 50% increase using AM 1.5G filtered light from the same solar simulator, although performances are about a quarter of those using open spectrum light. The *STH* performances of these samples reveal that these photoanodes are relevant in terms of water splitting behavior with respect to comparable samples/devices, taking into account also that these *STH* values refer to the behavior of thin film photoanodes in a full PEC device (without bias application) with separate compartments for H_2 and O_2 evolution, and not in hemicells or in power systems as often reported in literature.

The *IPCE* measurements (Fig. 10) clearly evidence that the presence of CuO nanoparticles induces an enhanced incident photon to current conversion efficiency in the 300–340 nm region. This result is well consistent with the performances of the system using open spectrum or AM 1.5G filtered light from the solar simulator. A quite consistent agreement is observed between results obtained in photocurrent density (both in chronoamperometric tests and measured in-situ during PEC experiments) and the behavior in H_2 photogeneration by water splitting. Moreover, a good stability in the behavior during the experiments was observed.

Except for a few larger particles located on the top surface of the TNT film, CuO is present as small nanoparticles of few nm inside the TiO_2 nanotubes, as shown by TEM (Fig. 4a) and SEM (Fig. 1) results. The TiO_2 nanotubes are well crystalline and present in the anatase crystalline form, with preferential exposition of the {001} facets, as shown by XRD results (Fig. 2). The presence of these CuO nanoparticles is responsible for the shift of the TiO_2 band gap from 3.2 to 2.8 eV (Fig. 5). For crystallites of about 20 nm, the band gap was observed at 2.5 eV with respect to the band gap of bulk CuO (1.2–1.9 eV) [68]. For the smaller CuO particles present in TNTs, the shift is expected at even shorter wavelengths, and thus well consistent with what experimentally observed (Fig. 5). Moreover, the clear tail in the absorption edge of band gap may be attributed to the presence of Cu_2O nanoparticles (see the dashed red line in Fig. 5b), evidencing an additional band gap energy of about 2.0 eV, in accordance with what reported in literature for Cu_2O (2.0–2.2 eV) [58]. However, diffuse reflectance data show that the enhanced absorption is mainly observed above about 400 nm, while *IPCE* measurements (Fig. 10) evidence that there is no effect of CuO/Cu_2O above about 400 nm. Thus, the small change in the band gap cannot be responsible of the enhanced performances, as often indicated in literature (see introduction).

Chronoamperometric results (Fig. 6) evidence the presence of an induction time upon illumination in reaching steady-state photocurrent density, and on the contrary a slight delay in reaching background value after switching off the light (Fig. 6b). The effect could be reasonably interpreted as the trapping of some photogenerated electrons during the initial stage of the photoinduced charge separation (e^-/h^+) process. This effect could promote the charge separation and thus the photocurrent density in the transition stage. Therefore, reasonably the interpretation is slightly different. In fact, the addition of electrons to CuO nanoparticles leads to the formation of p-type Cu_2O species [69] with the creation of p–n junctions between the Cu_xO nanoparticles and TNT. This transient generation of a p–n junction between the Cu_xO nanoparticles and TNT upon illumination is likely responsible for the enhanced charge separation and for the promoted behavior in water splitting.

The promotion effect due to the addition of transition metal nanoparticles to semiconductors is often interpreted as co-catalyst effect in promoting O_2 or H_2 evolution [18,70], although in our case of PEC cells only oxygen evolution is present in the photoanode. A co-catalysis role implies an acceleration of CuO in the rate of O_2 evolution by water photo-oxidation, which does not seem likely, but cannot be proved from our results. We could only remark that we observed a quite good correlation between photocurrent generation and performances in H_2 photogeneration. The interpretation of the formation of a p–n junction between the Cu_xO nanoparticles and TNT upon illumination is more consistent with our experimental results. The creation of a p–n junction when combining Cu_2O with an n-type semiconductor (such as TiO_2) is well reported in literature [71]. The superior photo-catalytic activity obtained in presence of a p–n junction is due to the presence of electrostatic field at the junction facilitating the charge separation between electrons and holes. Another mechanism often indicated to explain this promotion effect is the presence of a Schottky barrier, which requires the creation of a metal-semiconductor junction. However, we did not observe the formation of a Schottky barrier, neither it is reasonable to have metallic Cu under the strong oxidizing conditions of the photoanode (nascent oxygen). In addition, this CuO-TNT sample shows about a twice higher efficiency in H_2 photogeneration than a Cu-TNT sample earlier investigated [61].

In conclusion, CuO nanoparticles decorating TNT thin film photoanodes are effective in promoting water splitting reaction in a PEC cell both using open spectrum and AM 1.5G filtered light from a solar simulator, evidencing an increase in the performances of about 20 and 50%, respectively. Even if further work is needed to clarify these aspects, the improved performances of CuO-TNT electrode may be mainly associated to the transient generation of a p–n junction between the Cu_xO nanoparticles and TNT upon illumination, which enhances photocurrent density by promoting charge separation.

Acknowledgments

The authors would like to express their deepest gratitude and indebtedness to the Brazilian Research Assistance Agency – FAPESP

(2016/07895-1) for the financial support granted during this research. This paper was made in the frame of also the PRIN 2015 SMARTNESS project nr. 2015K7FZLH "Solar driven chemistry: new materials for photo- and electro-catalysis", which is gratefully acknowledged.

References

[1] P. Lianos, Review of recent trends in photoelectrocatalytic conversion of solar energy to electricity and hydrogen, Appl. Catal. B: Environ. 210 (2017) 235–254.
[2] N. Armaroli, V. Balzani, The hydrogen issue, ChemSusChem 4 (2011) 21–36.
[3] W. Wang, F. Li, D. Zhang, D.Y.C. Leung, G. Li, Photoelectrocatalytic hydrogen generation and simultaneous degradation of organic pollutant via CdSe/TiO_2 nanotube arrays, Appl. Surf. Sci. 362 (2016) 490–497.
[4] C. Ampelli, S. Perathoner, G. Centi, CO_2 utilization: an enabling element to move to a resource and energy efficient chemical and fuel production, Phil. Trans. R. Soc. A 373 (20140177) (2015) 1–35.
[5] C. Ampelli, C. Genovese, B.C. Marepally, G. Papanikolaou, S. Perathoner, G. Centi, Electrocatalytic conversion of CO_2 to produce solar fuels in electrolyte or electrolyte-less configurations of PEC cells, Faraday Discuss. 183 (2015) 125–145.
[6] C. Ampelli, C. Genovese, G. Centi, R. Passalacqua, S. Perathoner, Nanoscale engineering in the development of photoelectrocatalytic cells for producing solar fuels, Top. Catal. 59 (2016) 757–771.
[7] S. Perathoner, G. Centi, D. Su, Turning perspective in photoelectrocatalytic cells for solar fuel, ChemSusChem 9 (2016) 345–357.
[8] C. Ampelli, F. Tavella, S. Perathoner, G. Centi, Engineering of photoanodes based on ordered TiO $_2$-nanotube arrays in solar photo-electrocatalytic (PECa) cells, Chem. Eng. J. 320 (2017) 352–362.
[9] X. Ning, J. Li, B. Yang, W. Zhen, Z. Li, B. Tian, G. Lu, Inhibition of photocorrosion of CdS via assembling with thin film TiO_2 and removing formed oxygen by artificial gill for visible light overall water splitting, Appl. Catal. B: Environ. 212 (2017) 129–139.
[10] J. Yan, H. Wu, H. Chen, Ya Zhang, F. Zhang, S.F. Liu, Fabrication of TiO_2/C_3N_4 heterostructure for enhanced photocatalytic Z-scheme overall water splitting, Appl. Catal. B: Environ. 191 (2016) 130–137.
[11] J. Wang, J. Yang, Z. Zheng, T. Lu, W. Gao, The role of thin NiPi film for enhancing solar water splitting performance of Ti doped hematite, Appl. Catal. B: Environ. 218 (2017) 277–286.
[12] L.K. Preethi, T. Mathews, M. Nand, S.N. Jha, C.S. Gopinath, S. Dash, Band alignment and charge transfer pathway in three phase anatase-rutile-brookite TiO_2 nanotubes: an efficient photocatalyst for water splitting, Appl. Catal. B: Environ. 218 (2017) 9–19.
[13] S. Tanigawa, H. Irie, Visible-light-sensitive two-step overall water-splitting based on band structure control of titanium dioxide, Appl. Catal. B: Environ. 180 (2016) 1–5.
[14] P. Wang, S. Zhan, Y. Xia, S. Ma, Q. Zhou, Y. Li, The fundamental role and mechanism of reduced graphene oxide in rGO/Pt-TiO_2 nanocomposite for high-performance photocatalytic water splitting, Appl. Catal. B: Environ. 207 (2017) 335–346.
[15] G. Li, Z. Lian, W. Wang, D. Zhang, H. Li, Nanotube-confinement induced size-controllable g-C_3N_4 quantum dots modified single-crystalline TiO_2 nanotube arrays for stable synergetic photoelectrocatalysis, Nano Energy 19 (2016) 446–454.
[16] H. Pan, Principles on design and fabrication of nanomaterials as photocatalysts for water-splitting, Renew. Sust. Energy Rev. 57 (2016) 584–601.
[17] K. Ueno, T. Oshikiri, H. Misawa, Plasmon-Induced water splitting using metallic-Nanoparticle-Loaded photocatalysts and photoelectrodes, ChemPhysChem 17 (2016) 199–215.
[18] Y. Ma, X. Wang, Y. Jia, X. Chen, H. Han, C. Li, Titanium dioxide-Based nanomaterials for photocatalytic fuel generations, Chem. Rev. 114 (2014) 9987–10043.
[19] J.J. Brancho, B.M. Bartlett, Challenges in Co-Alloyed titanium oxynitrides, a promising class of photochemically active materials, Chem. Mat. 27 (2015) 7207–7217.
[20] S. Kment, F. Riboni, S. Pausova, L. Wang, L. Wang, H. Han, Z. Hubicka, J. Krysa, P. Schmuki, R. Zboril, Photoanodes based on TiO_2 and α-Fe_2O_3 for solar water splitting – superior role of 1D nanoarchitectures and of combined heterostructures, Chem. Soc. Rev. 46 (2017) 3716–3769.
[21] F. Wang, L. Song, H. Zhang, L. Luo, D. Wang, J. Tang, One-Dimensional metal-Oxide nanostructures for solar photocatalytic water-Splitting, J. Electronic Mat. 46 (2017) 4716–4724.
[22] M. Ge, Q. Li, C. Cao, J. Huang, S. Li, S. Zhang, Z. Chen, K. Zhang, S.S. Al-Deyab, Y. Lai, Water splitting one-dimensional TiO_2 nanotube photocatalysts for solar water splitting, Adv. Sci. 4 (2017), http://dx.doi.org/10.1002/advs.201770005 (1600152/1-31).
[23] X. Chen, Z. Zhang, L. Chi, A.K. Nair, W. Shangguan, Z. Jiang, Recent advances in visible-light-driven photoelectrochemical water splitting: catalyst nanostructures and reaction systems, Nano-Micro Lett. 8 (2016) 1–12.
[24] Z. Lian, W. Wang, S. Xiao, X. Li, Y. Cui, D. Zhang, G. Li, H. Li, Plasmonic silver quantum dots coupled with hierarchical TiO_2 nanotube arrays photoelectrodes for efficient visible-light photoelectrocatalytic hydrogen evolution, Sci. Rep. 5 (10461) (2015) 1–10.
[25] H. Li, Z. Li, Y. Yu, Y. Ma, W. Yang, F. Wang, X. Yin, X. Wang, Surface-plasmon-resonance-enhanced photoelectrochemical water splitting from Au-Nanoparticle-Decorated 3D TiO_2 nanorod architectures, J. Phys. Chem. C 121 (2017) 12071–12079.
[26] J. Zhang, X. Jin, P.I. Morales-Guzman, X. Yu, H. Liu, H. Zhang, L. Razzari, J.P. Claverie, Engineering the absorption and field enhancement properties of Au–TiO_2 nanohybrids via whispering gallery mode resonances for photocatalytic water splitting, ACS Nano 10 (2016) 4496–4503.
[27] P. Peerakiatkhajohn, T. Butburee, J.-H. Yun, H. Chen, R.M. Richards, L. Wang, A hybrid photoelectrode with plasmonic Au@TiO_2 nanoparticles for enhanced photoelectrochemical water splitting, J. Mat. Chem. A 3 (2015) 20127–20133.
[28] C. Ampelli, F. Tavella, C. Genovese, S. Perathoner, M. Favaro, G. Centi, Analysis of the factors controlling performances of Au-modified TiO_2 nanotube array based photoanode in photo-electrocatalytic (PECa) cells, J. Energy Chem. 26 (2017) 284–294.
[29] A. Paracchino, V. Laporte, K. Sivula, M. Grätzel, E. Thimsen, Highly active oxide photocathode for photoelectrochemical water reduction, Nature Mater. 10 (2011) 456–461.
[30] Z. Zhang, P. Wang, Highly stable copper oxide composite as an effective photocathode for water splitting via a facile electrochemical synthesis strategy, J. Mater. Chem. 22 (2012) 2456–2464.
[31] Q.-B. Ma, J.P. Hofmann, A. Litke, E.J.M. Hensen, Cu_2O photoelectrodes for solar water splitting: tuning photoelectrochemical performance by controlled faceting, Sol. Energy Mater. Sol. Cells 141 (2015) 178–186.
[32] K. Nakaoka, J. Ueyama, K. Ogura, Photoelectrochemical behavior of electrodeposited CuO and Cu2 O Thin films on conducting substrates, J. Electrochem. Soc. 151 (2004) C661–C665.
[33] M.J. Siegfried, K.-S. Choi, Conditions and mechanism for the anodic deposition of cupric oxide films in slightly acidic aqueous media, J. Electrochem. Soc. 154 (2007) D674–D677.
[34] K. Chiang, R. Amal, T. Tran, Photocatalytic degradation of cyanide using titanium dioxide modified with copper oxide, Adv. Environ. Res. 6 (2002) 471–485.
[35] J.F. De Brito, M. Valnice, B. Zanoni, On the application of Ti/TiO_2/CuO n-p junction semiconductor: a case study of electrolyte, temperature and potential influence on CO_2 reduction, Chem. Eng. J. 318 (2017) 264–271.
[36] Y. Liu, H. Zhou, J. Li, H. Chen, D. Li, B. Zhou, W. Cai, Enhanced photoelectrochemical properties of Cu_2O-loaded short TiO2 nanotube array electrode prepared by sonoelectrochemical deposition, Nano-Micro Lett. 2 (2010) 277–284.
[37] G.K. Mor, O.K. Varghese, R.H.T. Wilke, S. Sharma, K. Shankar, T.J. Latempa, K.-S. Choi, C.A. Grimes, P-Type Cu-Ti-O nanotube arrays and their use in self-Biased heterojunction photoelectrochemical diodes for hydrogen generatio, Nano Lett. 8 (2008) 1906–1911.
[38] F. Teng, M. Chen, N. Li, X. Hua, K. Wang, T. Xu, Effect of TiO_2 surface structure on the hydrogen production activity of the Pt@CuO/TiO_2 photocatalysts for water splitting, ChemCatChem 6 (2014) 842–847.
[39] Q. Hu, J. Huang, G. Li, J. Chen, Z. Zhang, Z. Deng, Y. Jiang, W. Guo, Y. Cao, Effective water splitting using CuO_x/TiO_2 composite films: role of Cu species and content in hydrogen generation, Appl. Surface Science 369 (2016) 201–206.
[40] S. Xu, A.J. Du, J. Liu, J. Ng, D.D. Sun, Highly efficient CuO incorporated TiO_2 nanotube photocatalyst for hydrogen production from water, Int. J. Hydrogen Energy 36 (2011) 6560–6568.
[41] H. Hou, M. Shang, F. Gao, L. Wang, Q. Liu, J. Zheng, Z. Yang, W. Yang, Highly efficient photocatalytic hydrogen evolution in ternary hybrid TiO_2/CuO/Cu thoroughly mesoporous nanofibers, ACS Appl. Mater. Interfaces 8 (2016) 20128–20137.
[42] Y.-H. Yu, Y.-P. Chen, Z. Cheng, Microwave-assisted synthesis of rod-like CuO/TiO_2 for high-efficiency photocatalytic hydrogen evolution, Int. J. Hydrogen Energy 40 (2015) 15994–16000.
[43] D.P. Kumar, M.V. Shankar, M.M. Kumari, G. Sadanandam, B. Srinivas, V. Durgakumari, Nano-size effects on CuO/TiO_2 catalysts for highly efficient H_2 production under solar light irradiation, Chem. Commun. 49 (2013) 9443–9445.
[44] C. Ampelli, C. Genovese, R. Passalacqua, S. Perathoner, G. Centi, The use of a solar photoelectrochemical reactor for sustainable production of energy, Theor. Found. Chem. Eng. 46 (2012) 651–657.
[45] C. Ampelli, G. Centi, R. Passalacqua, S. Perathoner, Electrolyte-less design of PEC cells for solar fuels: prospects and open issues in the development of cells and related catalytic electrodes, Catal. Today 259 (2016) 246–258.
[46] C. Ampelli, G. Centi, R. Passalacqua, S. Perathoner, Synthesis of solar fuels by a novel photoelectrocatalytic approach, Energy Environ. Sci. 3 (2010) 292–301.
[47] L. Perazolli, L. Nuñez, M.R. Apolinário da Silva, G.F. Pegler, A.G. Cavalarri Costalonga, R. Gimenes, M.M. Kondo, M.A. Zaghete Bertochi, TiO_2/CuO films obtained by citrate precursor method for photocatalytic application, Mater. Sci. Appl. 2 (2011) 564–571.
[48] C. Ampelli, R. Passalacqua, S. Perathoner, G. Centi, Development of a TiO_2 nanotube array-based photo-reactor for H_2 production by water splitting, Chem. Eng. Trans. 24 (2011) 187–192.
[49] Y. Dai, C.M. Cobley, J. Zeng, Y. Sun, Y. Xia, Synthesis of anatase TiO_2 nanocrystals with exposed {001} facets, Nano Lett. 9 (2009) 2455–2459.
[50] A.P. Moura, L.S. Cavalcante, J.C. Sczancoski, D.G. Stroppa, E.C. Paris, A.J. Ramirez, E. Longo, Structure and growth mechanism of CuO plates obtained by microwave-hydrothermal without surfactantsAdv, Powder. Technol. 21 (2010) 197–202.
[51] A.R. Kim, B. Lee, M. June, D. Ju, J. Wook, Catalytic performance on CuO–Cr_2O_3–Ga_2O_3 mixed oxides for water gas shift reaction: effects of Ga/Cr molar ratio, Catal. Commun. 19 (2012) 66–69.
[52] C. Zhu, A. Osherov, M.J. Panzer, Surface chemistry of electrodeposited Cu_2O films studied by XPS, Electrochim. Acta 111 (2013) 771–778.
[53] G. Centi, R. Passalacqua, S. Perathoner, D.S. Su, Oxide thin films based on ordered arrays of 1D nanostructure. A possible approach toward bridging material gap in catalysis, Phys. Chem. Chem. Phys. 9 (2007) 4930–4938.
[54] J. Tauc, R. Grigorovici, A. Vancu, Optical properties and electronic structure of amorphous germanium, Phys. Status Solidi 15 (1966) 627–637.
[55] G.G. Bessegato, J.C. Cardoso, M.V.B. Zanoni, Enhanced photoelectrocatalytic degradation of an acid dye with boron-doped TiO_2 nanotube anodes, Catal. Today 240

(2015) 100–106.
[56] Y.F. Lim, J.J. Choi, T. Hanrath, Facile synthesis of colloidal CuO nanocrystals for light-Harvesting applications, J. Nanomater. 2012 (2012) (393160/1-6).
[57] L. Jing, B. Xin, F. Yuan, L. Xue, B. Wang, H. Fu, Effects of surface oxygen vacancies on photophysical and photochemical processes of Zn-Doped TiO_2 nanoparticles and their relationships, J. Phys. Chem. B 110 (2006) 17860–17865.
[58] M. Hara, T. Kondo, M. Komoda, S. Ikeda, K. Shinohara, A. Tanaka, J.N. Kondo, K. Domen, Cu_2O as a photocatalyst for overall water splitting under visible light irradiation, Chem. Commun. (1998) 357–358.
[59] H. Yan, X. Wang, M. Yaon, X. Yao, Band structure design of semiconductors for enhanced photocatalytic activity: the case of TiO_2, Progr. Nat. Sci. − Mater. Int. 23 (2013) 402–407.
[60] I. Ganesh, P.P. Kumara, I. Annapoorna, J.M. Sumliner, M. Ramakrishna, N.Y. Hebalkar, G. Padmanabham, G. Sundararajan, Preparation and characterization of Cu-doped TiO_2 materials for electrochemical, photoelectrochemical, and photocatalytic applications, Appl. Surf. Sci. 293 (2014) 229–247.
[61] C. Ampelli, C. Genovese, F. Tavella, M. Favaro, S. Agnoli, G. Granozzi, S. Perathoner, G. Centi, Assembling of TiO_2 nanotube photoelectrodes with enhanced visible properties for a sustainable production of H_2, Chem. Eng. Trans. 43 (2015) 667–672.
[62] W. Shi, F. Guo, H. Wang, S. Guo, H. Li, Y. Zhou, C. Zhu, Y. Liu, H. Huang, B. Mao, Y. Liu, Z. Kanget, New insight of water-Splitting photocatalyst: H_2O_2-Resistance poisoning and photothermal deactivation in sub-micrometer CoO octahedrons, ACS Appl. Mater. Interfaces 9 (2017) 20585–20593.
[63] K. Welter, V. Smirnov, J.-P. Becker, P. Borowski, S. Hoch, A. Maljusch, W. Jaegermann, F. Finger, The influence of operation temperature and variations of the illumination on the performance of integrated photoelectrochemical water-splitting devices, ChemElectroChem 4 (2017) 1–11.
[64] P. Xu, J. Feng, T. Fang, X. Zhao, Z. Li, Z. Zou, Photoelectrochemical cell for unassisted overall solar water splitting using a $BiVO_4$ photoanode and Si nanoarray photocathode, RSC Adv. 6 (2016) 9905–9910.
[65] P.P. Patel, H.J. Jampani, O.I. Velikokhatnyi, M.K. Datta, D. Hong, B. Gattu, J.A. Poston, A. Manivannan, P.N. Kumta, Nitrogen and cobalt co-doped zinc oxide nanowires −Viable photoanodes for hydrogen generation via photoelectrochemical water splitting, J. Power Sources 299 (2015) 11–24.
[66] S. Kment, P. Schmuki, Z. Hubicka, L. Machala, R. Kirchgeorg, N. Liu, L. Wang, K. Lee, J. Olejnicek, M. Cada, I. Gregora, R. Zboril, ACS Nano 9 (2015) 7113–7123.
[67] J. Chen, D. Yang, D. Song, J. Jiang, A. Ma, M.Z. Hu, C. Ni, Recent progress in enhancing solar-to-hydrogen efficiency, J. Power Sources 280 (2015) 649–666.
[68] H.K. Ayask, J.V. Khaki, M.H. Sabzevar, Facile synthesis of copper oxide nanoparticles using copper hydroxide by mechanochemical process, J. Ultrafine Grained Nanostruct. Mat. 48 (2015) 37–44.
[69] L. Xiong, S. Huang, X. Yang, M. Qiu, Z. Chen, Y. Yu, p-Type and n-type Cu_2O semiconductor thin films: controllable preparation by simple solvothermal method and photoelectrochemical properties, Electrochim. Acta 56 (2011) 2735–2739.
[70] T. Jafari, E. Moharreri, A.S. Amin, R. Miao, W. Song, S.L. Suib, Photocatalytic water Splitting—the untamed dream: a review of recent advances, Molecules 21 (2016) (900/1-29).
[71] L. Sinatra, A.P. LaGrow, W. Peng, A.R. Kirmani, A. Amassian, H. Idriss, O.M. Bakr, A $Au/Cu_2O–TiO_2$ system for photo-catalytic hydrogen production. A pn-junction effect or a simple case of in situ reduction? J. Catal. 322 (2015) 109–117.